A Low Mach Number Model for Moist Atmospheric Flows

Max Duarte, Ann S. Almgren, John B. Bell

A Low Mach Number Model for Moist Atmospheric Flows

Max Duarte*, Ann S. Almgren, and John B. Bell
CCSE, Lawrence Berkeley National Laboratory, Berkeley, California

August 28, 2014

Abstract

We introduce a low Mach number model for moist atmospheric flows that accurately incorporates reversible moist processes in flows whose features of interest occur on advective rather than acoustic time scales. Total water is used as a prognostic variable, so that water vapor and liquid water are diagnostically recovered as needed from an exact Clausius–Clapeyron formula for moist thermodynamics. Unlike the pseudo–incompressible formulation, this model allows a general equation of state. Low Mach number models can be computationally more efficient than a fully compressible model, but the low Mach number formulation introduces additional mathematical and computational complexity because of the divergence constraint imposed on the velocity field. Here, latent heat release is accounted for in the source term of the constraint by estimating the rate of phase change based on the time variation of saturated water vapor subject to the thermodynamic equilibrium constraint. We numerically assess the validity of the low Mach number approximation for moist atmospheric flows by contrasting the low Mach number solution to reference solutions computed with a fully compressible formulation for a variety of test problems.

1 Introduction

Small–scale atmospheric phenomena are typically characterized by relatively slow dynamics, that is, low Mach number flows for which the fast acoustic modes are physically irrelevant. Thus, numerical modeling of these flows does not typically require explicitly resolving fast–propagating sound waves. Two different approaches have been widely used to remove the time step constraint that would result from resolving fast acoustic modes. The first and more common approach solves the fully compressible equations of motion but limits the impact of acoustic modes, for instance, by advancing the acoustic signal in time with an implicit time discretization or with multiple smaller time steps, as originally considered for cloud models in [TW76] and [KW78]. A second alternative consists of analytically filtering acoustic modes from the original compressible equations, thus deriving a new set of equations, often called sound–proof equations. Within this category are anelastic [Bat53, OP62, DF69, Gou69] and pseudo–incompressible [Dur89] models.

Several anelastic formulations (see, e.g., [Cla79, LH82, GS02]), and recently a pseudo–incompressible formalism ([OK14]), have been developed for moist flows. In this paper we derive a general low Mach number model for moist atmospheric flows using the low Mach number formalism in [ABNZ08] as a starting point. Analogously to [OK14] we consider only reversible processes given by water phase changes, using an exact Clausius–Clapeyron formula

* *Corresponding author address:* Max Duarte, Center for Computational Sciences and Engineering, Lawrence Berkeley National Laboratory, MS 50A-1148, 1 Cyclotron Rd. Berkeley, CA 94720
E-mail: MDGonzalez@lbl.gov

for moist thermodynamics. In contrast to [OK14], however, we derive the equations of motion in terms of conserved variables (like [Ooy90] in a compressible framework), that is, using appropriate invariant variables such that terms resulting from phase change are eliminated from the time evolution equations [Bet73, TC81, HH89]. We also include the effects of the specific heats of both water vapor and liquid water. Although the low Mach number formulation holds for any moist equation of state, for the purposes of numerical comparison with compressible solutions we consider the special case where both dry air and water vapor are assumed to be ideal gases.

While the larger time step allowed by the low Mach number formulation can lead to greater computational efficiency than a purely compressible formulation, it may also introduce larger errors in the dynamics of moist flows as investigated in [DAB$^+$14]. In addition to the latent heat release accompanying phase changes, thermodynamic properties such as the specific heat of moist air, as well as thermodynamic variables such as temperature, depend on the composition of the moist air, thus change over the time step. This motivates our use of invariant variables as prognostic variables, namely total water content and a specific enthalpy of moist air that accounts for both sensible and latent heats. In models where source terms related to phase transition appear explicitly in the evolution equations, they are typically first neglected or lagged in time and then corrected or estimated during a given time step; the use of invariant variables removes the need of accounting for such terms. Nevertheless, the diabatic contribution of the latent heat release must appear in the source term for the low Mach divergence constraint on the velocity field. In practice the latter involves computing the rate of evaporation (or condensation). Since no analytical expression exists for this rate, one of the most common ways to estimate it deduces it from the change in water vapor content necessary to ensure that there is no supersaturated water vapor at the end of the time step (cf. [SO73]). This variation is measured with respect to an initial estimate of water vapor that does not necessarily respect the saturation requirements either because it was initially advected without accounting for phase changes (see, e.g., [KW78, GS90, BF02, Sat03, OK14]) or because it considers a lagged evaporation rate from the previous time step (see, e.g., [GS02]). In our model, because water vapor is not used as a prognostic variable, we cannot compute this variation of water vapor. Instead we adopt a different approach, similar to [LH82], that estimates the evaporation rate based on the fact that whenever a parcel is saturated, a Clausius–Clapeyron formula relates the local values of water content to the thermodynamics within the parcel. The conservation equation for saturated water vapor then becomes a time–varying constraint that guarantees thermodynamic equilibrium from which the evaporation rate can be estimated. The latter is thus computed as required during a time step using the water content and thermodynamic variables diagnostically recovered from the invariant prognostic variables.

This paper is organized as follows. We introduce the new low Mach number model for moist atmospheric flows in Section 2, and describe the moist thermodynamics in Section 3. In Section 4 we discuss the numerical implementation. Finally, in Section 5, we present several numerical comparisons and discuss our findings.

2 Low Mach number formulation

We begin by writing the fully compressible equations of motion expressing conservation of mass, momentum, and enthalpy in a constant gravitational field in which we neglect Coriolis

forces and viscous terms:

$$\frac{\partial \rho}{\partial t} + \boldsymbol{\nabla} \cdot (\rho \boldsymbol{U}) = 0, \tag{1}$$

$$\frac{\partial (\rho \boldsymbol{U})}{\partial t} + \boldsymbol{\nabla} \cdot (\rho \boldsymbol{U}\boldsymbol{U}) + \boldsymbol{\nabla} p = -\rho g \hat{\boldsymbol{e}}_z, \tag{2}$$

$$\frac{\partial (\rho \widehat{h})}{\partial t} + \boldsymbol{\nabla} \cdot (\rho \widehat{h} \boldsymbol{U}) - \frac{Dp}{Dt} = \rho \mathcal{H}, \tag{3}$$

where the material derivative is defined as $D/Dt = \partial/\partial t + \boldsymbol{U} \cdot \boldsymbol{\nabla}$. Here ρ is the total density, $\boldsymbol{U}$ is the velocity, and $\widehat{h}$ is the specific enthalpy of moist air. The pressure, p, is defined by an equation of state (EOS). The term $\mathcal{H}$ represents a source of heat (per unit mass and time) to the system, such as thermal conduction or radiation. We include gravitational acceleration given by $\boldsymbol{g} = -g\hat{\boldsymbol{e}}_z$, where $\hat{\boldsymbol{e}}_z$ is the unit vector in the vertical direction.

We then follow the formalism as in [Rom08] for moist atmospheres with the additional simplification that at any grid point all phases have the same temperature and velocity. Here we also ignore ice–phase microphysics, precipitation fallout, and subgrid–scale turbulence. We consider an atmosphere with three components, dry air, water vapor, and liquid water, and treat moist air as an ideal mixture with the water phases in thermodynamic equilibrium, so that only reversible processes are taken into account. Denoting by q_a, q_v, and q_l the mass fraction of dry air, water vapor, and liquid water, respectively, we write

$$\frac{\partial (\rho q_a)}{\partial t} + \boldsymbol{\nabla} \cdot (\rho q_a \boldsymbol{U}) = 0, \tag{4}$$

$$\frac{\partial (\rho q_v)}{\partial t} + \boldsymbol{\nabla} \cdot (\rho q_v \boldsymbol{U}) = e_v, \tag{5}$$

$$\frac{\partial (\rho q_l)}{\partial t} + \boldsymbol{\nabla} \cdot (\rho q_l \boldsymbol{U}) = -e_v. \tag{6}$$

Recall that ρ is the total density and thus includes dry air, water vapor, and liquid water; furthermore, $q_a + q_v + q_l = 1$. The evaporation rate, e_v, has dimensions of mass per volume per time; negative values of e_v correspond to condensation. However, introducing the mass fraction of total water, $q_w = q_v + q_l$, here we will consider

$$\frac{\partial (\rho q_w)}{\partial t} + \boldsymbol{\nabla} \cdot (\rho q_w \boldsymbol{U}) = 0, \tag{7}$$

instead of equations (5)–(6). (We note that the system including both (1) and (4)–(6) or (1), (4), and (7) is over–specified; in practice (1) need not be solved separately.)

The constant–volume specific heat of moist air is given by

$$c_{vm} = q_a c_{va} + q_v c_{vv} + q_l c_{vl},$$

with the specific heats at constant volume: c_{va}, c_{vv}, and c_{vl}, for dry air, water vapor, and liquid water, respectively. The internal energy of moist air, $\widehat{e}$, can be thus defined as in [Rom08],

$$\widehat{e} = c_{vm} (T - T_{\text{trip}}) + q_v E_{0v}, \tag{8}$$

where T_{trip} is the triple–point temperature and E_{0v} is the specific internal energy of water vapor at the triple point, while the enthalpy of moist air is given by

$$\widehat{h} = \widehat{e} + \frac{p}{\rho}. \tag{9}$$

Note that an evolution equation for the internal energy

$$\frac{\partial\left(\rho\widehat{e}\right)}{\partial t}+\boldsymbol{\nabla}\cdot\left(\rho\widehat{e}\boldsymbol{U}\right)+p\left(\boldsymbol{\nabla}\cdot\boldsymbol{U}\right)=\rho\mathcal{H}, \tag{10}$$

can be used instead of (3). In either case, there are no source terms related to phase change in (3) or (10), as observed in [Ooy90] and [DAB$^+$14]. Finally, an equation of state for moist air must be provided to close the system given by (1)–(4) with (7). Let us consider a general EOS written as $p=p(\rho,T,q_a,q_v,q_l)$. (Because $q_a+q_v+q_l=1$ we could remove one of these three arguments from the equation of state; for clarity of exposition, however, we leave all three.)

Following the nondimensional analysis performed in [ABRZ06a] for low Mach number (M) flows, we can decompose the pressure, $p(\boldsymbol{x},t)$, $\boldsymbol{x}=(x,y,z)$, into a base state pressure, $p_0(z,t)$, and a perturbational, or dynamic, pressure, $p'(\boldsymbol{x},t)$, such that $|p'|/p_0=O(M^2)$. In contrast to anelastic models, the perturbations in density and temperature themselves need not be small for the equations to remain valid. The base state is assumed to be in hydrostatic equilibrium, i.e., $\boldsymbol{\nabla}p_0=-\rho_0 g\hat{\boldsymbol{e}}_z$, where $\rho_0=\rho_0(z,t)$ is the base state density. The fully compressible momentum equation (2) could be rewritten as

$$\frac{\partial\left(\rho\boldsymbol{U}\right)}{\partial t}+\boldsymbol{\nabla}\cdot\left(\rho\boldsymbol{U}\boldsymbol{U}\right)+\boldsymbol{\nabla}p'=-(\rho-\rho_0)g\hat{\boldsymbol{e}}_z \tag{11}$$

with no approximation. The low Mach number momentum equation, however, in order to enforce conservation of a low Mach number form of total energy, has the form

$$\frac{\partial\left(\rho\boldsymbol{U}\right)}{\partial t}+\boldsymbol{\nabla}\cdot\left(\rho\boldsymbol{U}\boldsymbol{U}\right)+\boldsymbol{\nabla}p'=-(\rho-\rho_0)g\hat{\boldsymbol{e}}_z-\left(\frac{\rho_0}{\rho}\left.\frac{\partial\rho}{\partial p_0}\right|_s p'\right)g\hat{\boldsymbol{e}}_z, \tag{12}$$

as introduced by [KP12]. Here the derivative of ρ with respect to p_0 is taken at constant entropy, and is based on the low Mach number form of the equation of state, i.e. $p_0(z,t)=p(\rho,T,q_a,q_v,q_l)$. As pointed out in [VLB$^+$13], this form of the momentum equation is analytically equivalent to the momentum equation in the pseudo–incompressible equation set, i.e.,

$$\frac{\partial\boldsymbol{U}}{\partial t}+\boldsymbol{U}\cdot\boldsymbol{\nabla}\boldsymbol{U}+c_p\theta\boldsymbol{\nabla}\pi'=\frac{\theta-\theta_0}{\theta_0}g\hat{\boldsymbol{e}}_z \tag{13}$$

with Exner pressure, $\pi=(p/p_{00})^{R_a/c_{pa}}$ (p_{00} is a reference pressure, while R_a and c_{pa} stand for the specific gas constant and constant–pressure specific heat of dry air, respectively), potential temperature, $\theta=T/\pi$, and the base state potential temperature, θ_0, if we define a linearized relationship between the perturbational pressures, p' and π'.

To complete the low Mach number model for moist atmospheric flows we first replace p by p_0 in the equation of state. We then differentiate the equation along particle paths. Substituting expressions from the evolution equations leads to a constraint on the divergence of the velocity field which retains compressibility effects from stratification as well as latent heat release and compositional changes. Following the derivation in [ABNZ08], with details as given in Appendix A, we derive the following divergence constraint for the low Mach number model:

$$\boldsymbol{\nabla}\cdot\boldsymbol{U}+\alpha\frac{Dp_0}{Dt}=S, \tag{14}$$

with

$$\alpha=\frac{1}{\Gamma_1 p_0},\qquad S=\left[\frac{1}{\rho p_\rho}\left(p_{q_v}-p_{q_l}\right)-\sigma\left(\widehat{h}_{q_v}-\widehat{h}_{q_l}\right)\right]\frac{e_v}{\rho}+\sigma\mathcal{H}, \tag{15}$$

where $p_\rho = \partial p/\partial\rho|_{T,q_i}$, $p_T = \partial p/\partial T|_{\rho,q_i}$, $p_{q_i} = \partial p/\partial q_i|_{\rho,T,(q_j,j\neq i)}$, $\widehat{h}_p = \partial\widehat{h}/\partial p|_{T,q_i}$, $\widehat{h}_{q_i} = \partial\widehat{h}/\partial q_i|_{T,p,(q_j,j\neq i)}$, $\Gamma_1 = d(\log p)/d(\log\rho)|_s$, and $\sigma = p_T/\left(\rho c_{pm} p_\rho\right)$, where $c_{pm} = \partial\widehat{h}/\partial T|_{p,q_i}$ is the specific heat of moist air at constant pressure.

Summarizing the low Mach number equation set for moist atmospheric flows in the form we will use, we have

$$\frac{\partial(\rho q_a)}{\partial t} = -\boldsymbol{\nabla}\cdot(\rho q_a \boldsymbol{U}) \tag{16}$$

$$\frac{\partial(\rho q_w)}{\partial t} = -\boldsymbol{\nabla}\cdot(\rho q_w \boldsymbol{U}) \tag{17}$$

$$\frac{\partial(\rho\widehat{h})}{\partial t} = -\boldsymbol{\nabla}\cdot(\rho\widehat{h}\boldsymbol{U}) + \frac{Dp_0}{Dt} + \rho\mathcal{H}, \tag{18}$$

$$\frac{\partial \boldsymbol{U}}{\partial t} = -\boldsymbol{U}\cdot\boldsymbol{\nabla}\boldsymbol{U} - \frac{1}{\rho}\boldsymbol{\nabla}p' - \frac{(\rho-\rho_0)}{\rho}g\hat{\boldsymbol{e}}_z - \left(\frac{\rho_0}{\rho^2}\left.\frac{\partial\rho}{\partial p_0}\right|_s p'\right) g\hat{\boldsymbol{e}}_z, \tag{19}$$

$$\boldsymbol{\nabla}\cdot\boldsymbol{U} = -\alpha\frac{Dp_0}{Dt} + S, \tag{20}$$

where the total mass density is defined as

$$\rho = \rho q_a + \rho q_w. \tag{21}$$

An underlying assumption in the low Mach number approximation is that the pressure remains close to the background pressure. Heat release and large–scale convective motions in a convectively unstable background can both cause the background state to evolve in time. As discussed in [Alm00] and demonstrated numerically in [ABRZ06b] for an externally specified heating profile, if the base state does not evolve in response to heating, the low Mach number method quickly becomes invalid. For the small–scale motions of interest here, the base state can effectively be viewed as independent of time; however, for the sake of completeness we retain the full time dependence of the base state in the development of the methodology.

3 Moist thermodynamics

To define α and S according to (15) in the divergence constraint (20), we here consider dry air and water vapor to be ideal gases (see, e.g., [Ooy90, Sat03, KSD07]), and note that while the low Mach number formulation allows a more general equation of state, this is a standard assumption in atmospheric modeling. The partial pressures of dry air and water vapor are then given by $p_a = \rho q_a R_a T$ and $p_v = \rho q_v R_v T$, where R_a and R_v are the specific gas constants for dry air and water vapor, respectively. Denoting by M_a and M_v the molar masses of dry air and water, respectively, we know that $R_a = R/M_a$ and $R_v = R/M_v$, where R is the universal gas constant for ideal gases. If we define the specific gas constant of moist air as

$$R_m = q_a R_a + q_v R_v = \left(\frac{q_a}{M_a} + \frac{q_v}{M_v}\right) R, \tag{22}$$

then the sum of the partial pressures defines the total pressure of a parcel,

$$p = p_a + p_v = \rho R_m T. \tag{23}$$

Additionally, the specific heat capacities at constant pressure can be defined as

$$c_{pa} = c_{va} + R_a, \quad c_{pv} = c_{vv} + R_v, \quad c_{pm} = c_{vm} + R_m, \tag{24}$$

for dry air, water vapor, and moist air, respectively. A common approximation in cloud models is to neglect the specific heats of water vapor and liquid water (see, e.g., [BF02] for a study and discussion on this topic). Here we consider specific heats for all three phases.

With this choice for the equation of state for moist air (eq. (23)), we have

$$\alpha = \frac{1}{\gamma_m p_0}, \qquad S = \left[\frac{1}{(\epsilon q_a + q_v)} - \frac{L_e}{c_{pm}T}\right]\frac{e_v}{\rho} + \left[\frac{1}{c_{pm}T}\right]\mathcal{H}, \tag{25}$$

where $\gamma_m = c_{pm}/c_{vm}$ is the isentropic expansion factor of moist air, $\epsilon = R_a/R_v = M_v/M_a$, and the latent heat of vaporization, L_e, is defined as

$$L_e = E_{0v} + R_v T + (c_{vv} - c_{vl})(T - T_{\text{trip}}). \tag{26}$$

Note that both α and S depend on the composition of the moist mixture even if $e_v = 0$. We can now replace Γ_1 as used in (14)–(15) by γ_m for moist atmospheric flows.

The saturation vapor pressure with respect to liquid water, p_v^*, is defined by the following Clausius–Clapeyron relation:

$$p_v^*(T) = p_{\text{trip}}\left(\frac{T}{T_{\text{trip}}}\right)^{\alpha_v}\exp\left[\beta_v\left(\frac{1}{T_{\text{trip}}} - \frac{1}{T}\right)\right], \tag{27}$$

with constants α_v and β_v, given, for instance, by

$$\alpha_v = \frac{c_{pv} - c_{vl}}{R_v}, \qquad \beta_v = \frac{E_{0v} - (c_{vv} - c_{vl})T_{\text{trip}}}{R_v}, \tag{28}$$

as in [Rom08]. The saturated mass fraction of water vapor, q_v^*, can be then computed from the EOS, given in this case by

$$q_v^*(\rho, T) = \frac{p_v^*}{\rho R_v T}, \tag{29}$$

or equivalently by

$$q_v^*(q_a, p, T) = \frac{\epsilon q_a p_v^*}{p - p_v^*}. \tag{30}$$

Following [Ooy90, Sat03], we assume that air parcels cannot be supersaturated, and thus q_v cannot exceed its saturated value, q_v^*. The water mass fractions, q_v and q_l, as well as the temperature T, which are not explicitly computed in (16)–(20), are obtained by solving the following nonlinear system of equations:

$$\left.\begin{aligned} &\widehat{h} = c_{pm}(q_a, q_v, q_l)\,(T - T_{\text{trip}}) + R_m(q_a, q_v)T_{\text{trip}} + q_v E_{0v}, \\ &q_v = \min\left[q_v^*(\rho, T), q_w\right], \\ &q_l = q_w - q_v, \end{aligned}\right\} \tag{31}$$

which satisfies the Clausius–Clapeyron relation and the saturation requirements, given $(\rho, \widehat{h}, q_a, q_w)$.

Taking into account that the evaporation rate e_v is different from zero only when a change of phase is taking place, that is, when $q_v = q_v^*$, we can rewrite the conservation equation for q_v (eq. (5)) as

$$e_v = \frac{\partial\left(\rho q_v^*\right)}{\partial t} + \boldsymbol{\nabla}\cdot\left(\rho q_v^* \boldsymbol{U}\right) = \rho\frac{Dq_v^*}{Dt}. \tag{32}$$

We show in Appendix B that if $q_v = q_v^*$, then

$$e_v = \mathcal{A}_e \boldsymbol{\nabla}\cdot\boldsymbol{U} + \mathcal{B}_e\frac{Dp_0}{Dt} + \mathcal{C}_e\rho\mathcal{H}, \tag{33}$$

where parameters $\mathcal{A}_e$, $\mathcal{B}_e$, and $\mathcal{C}_e$ are in general functions of (ρ, T, q_a, q_v, q_l). Otherwise, $e_v = 0$ whenever $q_v < q_v^*$. In [LH82], the term $\boldsymbol{\nabla} \cdot (\rho q_v^* \boldsymbol{U})$ in (32) is replaced with $\boldsymbol{\nabla} \cdot (\rho q_{va} \boldsymbol{U})$, where (ρq_{va}) stands for the water vapor content advected without considering the evaporation rate in (5): $\partial(\rho q_{va})/\partial t + \boldsymbol{\nabla} \cdot (\rho q_{va} \boldsymbol{U}) = 0$.

Finally, using (32) to estimate e_v in S (eq. (25)) involves a low Mach divergence constraint where the source term depends on the pressure and the velocity field, i.e.,

$$\boldsymbol{\nabla} \cdot \boldsymbol{U} + \alpha \frac{Dp_0}{Dt} = S\left(\boldsymbol{\nabla} \cdot \boldsymbol{U}, \frac{Dp_0}{Dt}\right). \tag{34}$$

A simpler expression can be obtained by rearranging the terms in (34), as shown in Appendix C, which leads to a modified divergence constraint:

$$\boldsymbol{\nabla} \cdot \boldsymbol{U} + \widetilde{\alpha} \frac{Dp_0}{Dt} = \widetilde{S}, \tag{35}$$

similar to the general low Mach divergence constraint (14), with

$$\widetilde{\alpha} = \frac{1}{\widetilde{\gamma}_m p_0}, \qquad \widetilde{S} = \widetilde{\sigma} \mathcal{H}, \tag{36}$$

both depending on (ρ, T, q_a, q_v, q_l). In particular if no heat source is considered, we have that $\widetilde{S} = 0$ and all the information related to phase change is included in $\widetilde{\alpha}$. Now Γ_1 in the general low Mach constraint (14)–(15) is given by a modified isentropic expansion factor of moist air: $\widetilde{\gamma}_m$ (eq. (76) in Appendix C). Both divergence constraints, (34) and (35), are analytically equivalent.

4 Numerical methodology

In order to solve the low Mach number equation set (16)–(20) we begin with the MAESTRO code, which was originally designed to simulate low Mach number stratified, reacting flows in astrophysical settings [ABRZ06a, ABRZ06b, ABNZ08, NAB+10].

We recall that for the moist equation of state considered here we replace Γ_1 in the original MAESTRO notation by γ_m. Since γ_m in general varies in space and time, the solution procedure in the original MAESTRO algorithm replaces $\gamma_m(\boldsymbol{x})$ by $\overline{\gamma}_m(z)$, that is, $\alpha(z) = 1/(\overline{\gamma}_m p_0)$ in the divergence constraint (34) where $\overline{\gamma}_m$ is the lateral average of γ_m,

$$\overline{\gamma}_m(z) = \frac{1}{A(\Omega_H)} \int_{\Omega_H} \gamma_m(\boldsymbol{x})\, d\Omega, \tag{37}$$

where $\mathrm{A}(\Omega_H) = \int_{\Omega_H} d\Omega$, Ω_H is a region at constant height for the plane–parallel atmosphere, and $d\Omega$ represents an area measure. The same follows for $\widetilde{\gamma}_m$ in the modified divergence constraint (35): $\widetilde{\alpha}(z) = 1/(\overline{\widetilde{\gamma}}_m p_0)$. The introduction of an averaged γ_m (or $\widetilde{\gamma}_m$) allows us to rewrite the constraint (34) (or (35)) as

$$\boldsymbol{\nabla} \cdot (\beta_0 \boldsymbol{U}) = \beta_0 \left(S - \alpha \frac{\partial p_0}{\partial t}\right), \tag{38}$$

as shown in [ABRZ06a] (Appendix B), with

$$\beta_0(z,t) = \beta(0,t) \exp\left(\int_0^z \alpha(z) \frac{\partial p_0}{\partial z'}\, dz'\right), \tag{39}$$

(with $\widetilde{S}$ and $\widetilde{\alpha}$ instead of S and α if the modified divergence (35) is considered). Moreover, the momentum equation (19), including the correction term introduced by [KP12], can be equivalently recast as

$$\frac{\partial \boldsymbol{U}}{\partial t} = -\boldsymbol{U}\cdot\boldsymbol{\nabla}\boldsymbol{U} - \frac{\beta_0}{\rho}\boldsymbol{\nabla}\left(\frac{p'}{\beta_0}\right) - \frac{(\rho-\rho_0)}{\rho}g\hat{\boldsymbol{e}}_z, \tag{40}$$

as derived in [VLB+13], and discussed in [ABNZ].

MAESTRO thus solves the low Mach equation set (16)–(18) with the momentum equation (40) and the divergence constraint (38). A predictor–corrector formalism is implemented to solve the flow dynamics, as detailed in [NAB+10]. In the predictor step an estimate of the expansion of the base state is first computed, and then an estimate of the flow variables at the new time level. In the corrector step results of the previous state update are used to compute a new base state update as well as the full state update.

Since we are considering the time evolution of total water (17) and the definition of enthalpy of moist air (3) involves a conservation equation (18) without source terms related to phase change, all the information related to variations in the moist composition and latent heat release is contained in the divergence constraint (38). Here q_v and q_l, as well as the local temperature T, must be computed point–wise in order to define α, S, and β_0 (or $\widetilde{\alpha}$, $\widetilde{S}$, and β_0). Point–wise values of (q_v, q_l, T) are thus diagnostically recovered by solving the nonlinear system (31), given the values of $(\rho, \widehat{h}, q_a, q_w)$; we use the Newton solver described in [DAB+14].

We consider two approaches for handling phase transitions depending on which divergence constraint is used to define (38) in the numerical implementation: (34) or (35). In the first case, which uses (34), the evaporation rate is evaluated according to (33) and introduced in the source term S of the constraint. As previously remarked, there is a dependence of S on the velocity field and the base state pressure. Consequently, approximate or lagged values of $\boldsymbol{U}$ and p_0 are used to estimate e_v during the prediction step, which is later recomputed with the updated values of $\boldsymbol{U}$ and p_0 during the correction step. Notice, however, that during both steps the moist composition and hence phase transitions are diagnostically recovered based on the current values of $(\rho, \widehat{h}, q_a, q_w)$. The second approach consists of considering the modified divergence constraint (35), in which case there is no need to estimate the evaporation rate (33). Parameters $\widetilde{\alpha}$, $\widetilde{S}$, and β_0 in (38) are computed with (ρ, T, q_a, q_v, q_l) given the current values of $(\rho, \widehat{h}, q_a, q_w)$ throughout the predictor–corrector scheme for the flow dynamics.

The replacement of $\Gamma_1(\boldsymbol{x}, t)$ by its lateral average $\overline{\Gamma}_1(z, t)$ was demonstrated in [ABNZ08] to have little effect on the astrophysical flows studied there. In the case of moist atmospheric flows, Γ_1 is given by γ_m which varies according to the local moist air composition at a given time and position. If the modified divergence constraint (35) is considered, Γ_1 is given by $\widetilde{\gamma}_m$ which varies not only according to the moist air composition but also the local values of (ρ, T). We can thus consider the effects of localized variations in Γ_1 following [ABNZ08], by writing $\Gamma_1(\boldsymbol{x}, t) = \overline{\Gamma}_1(z, t) + \delta\Gamma_1(\boldsymbol{x}, t)$, and hence,

$$\boldsymbol{\nabla}\cdot\boldsymbol{U} = -\frac{1}{(\overline{\Gamma}_1 + \delta\Gamma_1)p_0}\frac{Dp_0}{Dt} + S, \tag{41}$$

instead of (20). Assuming that $\delta\Gamma_1 \ll \overline{\Gamma}_1$, we then have

$$\boldsymbol{\nabla}\cdot\boldsymbol{U} = -\frac{1}{\overline{\Gamma}_1 p_0}\frac{Dp_0}{Dt} + S + \frac{\delta\Gamma_1}{\overline{\Gamma}_1^2 p_0}\frac{Dp_0}{Dt}, \tag{42}$$

which leads to

$$\boldsymbol{\nabla}\cdot(\beta_0\boldsymbol{U}) = \beta_0\left(S - \alpha\frac{\partial p_0}{\partial t} + \frac{\delta\Gamma_1}{\overline{\Gamma}_1^2 p_0}\frac{Dp_0}{Dt}\right). \tag{43}$$

We will refer to the $\delta\Gamma_1$–correction whenever (43) is considered instead of (38). Notice that $Dp_0/Dt = \partial p_0/\partial t + \boldsymbol{U}\cdot\boldsymbol{\nabla}p_0$, and therefore, to solve (43) a lagged $\boldsymbol{U}$ is used in evaluating the right–hand side, as described in [ABNZ08].

5 Numerical simulations

We consider the benchmark problem proposed in [BF02] for moist flows, along with the corresponding configuration for dry air originally presented in [WS98]. Results will be compared with those obtained in [BF02] to first validate our numerical implementation. Then, they will be contrasted to those obtained using a fully compressible formulation according to [DAB$^+$14] We will see that a very good agreement is achieved in general using the low Mach number model for moist atmospheric flows. Both the first and second approach to implementing phase transitions are investigated. A second configuration based on [GC91] will also be studied for non–isentropic background states and both saturated and only partially saturated media, to further assess the low Mach number model. Finally, we will show a comparison of low Mach number to compressible simulations in three dimensions.

5.1 Numerical validation

Solutions of a benchmark test case are investigated in [BF02]. We aim at validating our numerical implementation by showing that our code provides qualitatively similar results for the same benchmark problem. The model in [BF02] considers fully compressible equations, where the conservation equations for vapor and liquid water are written in terms of the water vapor and cloud mixing ratios: $r_v = q_v/q_a$ and $r_c = q_l/q_a$, respectively. Additionally, the following equation is considered

$$\rho c_{vm}\left(\frac{\partial T}{\partial t} + \boldsymbol{U}\cdot\boldsymbol{\nabla}T\right) = -p\,(\boldsymbol{\nabla}\cdot\boldsymbol{U}) - (L_v - R_vT)e_v, \tag{44}$$

instead of a conservation equation for enthalpy (3), where the latent heat of vaporization, L_v, is defined as

$$L_v = L_{v0} - (c_{pl} - c_{pv})(T - T_0), \tag{45}$$

with constant reference values of L_v and T: L_{v0} and T_0, respectively. A nondimensional Exner pressure, π, and the potential temperature, θ, are used in [BF02], defined as

$$\pi = \left(\frac{p}{p_{00}}\right)^{R_a/c_{pa}}, \qquad \theta = \frac{T}{\pi}, \tag{46}$$

where $p_{00} = 1000\,\mathrm{mb}$. All this amounts to considering time dependent equations for $(\boldsymbol{U}, \pi, \theta, r_v, r_c)$, where the evaporation rate, e_v, appears in the source terms for π, θ, r_v, and r_c. The hydrostatic base state pressure can be found through

$$\frac{d\pi_0}{dz} = -\frac{g}{c_{pa}\theta_{\rho 0}}, \tag{47}$$

where subscript 0 stands for hydrostatic base quantities, and the density potential temperature, θ_ρ, is defined as

$$\theta_\rho = \theta\frac{(1 + r_v/\epsilon)}{(1 + r_t)}, \tag{48}$$

with the total water mixing ratio: $r_t = q_w/q_a$.

For the computations we consider the following constant parameters, taken from [BF02]: $R_a = 287\,\mathrm{J\ kg^{-1}\ K^{-1}}$, $R_v = 461\,\mathrm{J\ kg^{-1}\ K^{-1}}$, $L_{v0} = 2.5 \times 10^6\,\mathrm{J\ kg^{-1}}$, $c_{va} = 717\,\mathrm{J\ kg^{-1}\ K^{-1}}$, $c_{vv} = 1424\,\mathrm{J\ kg^{-1}\ K^{-1}}$, $c_{pl} = 4186\,\mathrm{J\ kg^{-1}\ K^{-1}}$, $T_0 = 273.15\,\mathrm{K}$, and $g = 9.81\,\mathrm{m\ s^{-1}}$. The remaining parameters used in our model are defined such that we have the same definition of the latent heat of vaporization, that is, $L_v = L_e$ from (45) and (26). Therefore we just need to consider: $T_{\mathrm{trip}} = T_0$, $c_{vl} = c_{pl}$, and $E_{0v} = L_{v0} - R_v T_{\mathrm{trip}}$. The saturation vapor pressure is computed with the Clausius–Clapeyron equation (27) with constants: $\alpha_v = 0$ and $\beta_v = L_{v0}/R_v$, with $p_{\mathrm{trip}} = 611\,\mathrm{Pa}$, taken from [OK14] that considers the same benchmark problem.

5.1.1 The Dry Simulation

Following [WS98] and [BF02], we consider a two–dimensional computational domain with height 10 km and width 20 km. The initial atmospheric environment is defined by a constant potential temperature of $\theta_0 = 300\,\mathrm{K}$, and the pressure field is obtained by integrating the hydrostatic equation (47) upwards. A warm perturbation is introduced in the domain, given by

$$\theta' = 2\cos^2\left(\frac{\pi L}{2}\right), \tag{49}$$

where

$$L = \min\left\{1, \sqrt{\left(\frac{x - x_c}{x_r}\right)^2 + \left(\frac{z - z_c}{z_r}\right)^2}\right\}, \tag{50}$$

with $x_c = 10\,\mathrm{km}$, $z_c = 2\,\mathrm{km}$, and $x_r = z_r = 2\,\mathrm{km}$. Note that while our formulation does not use the θ–π formalism, the expressions in (46) are used for the conversions, while the initial perturbation (49) is applied at constant pressure $p_0(z)$. We impose zero normal velocities on all four boundaries. For the thermodynamic variables, we impose homogeneous Neumann boundary conditions on the horizontal sides; the background state is reconstructed by extrapolation at vertical boundaries in order to determine the corresponding fluxes.

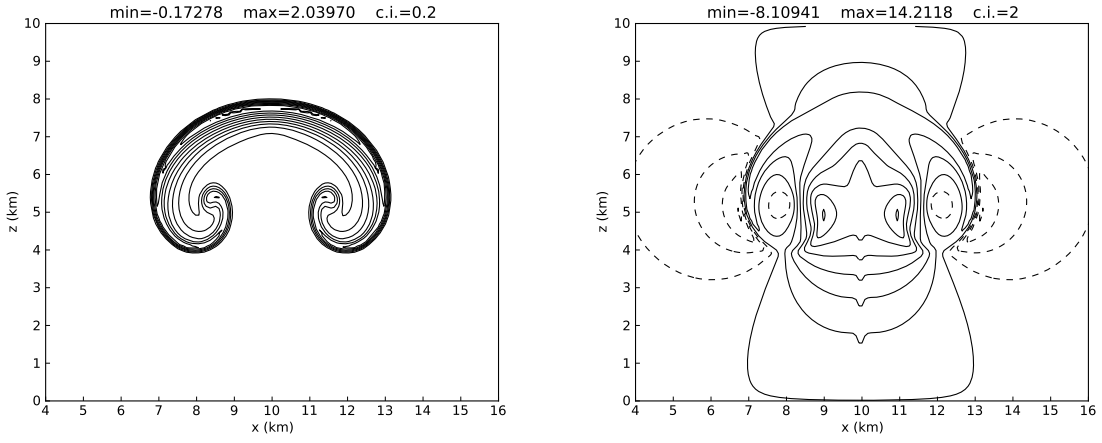

Figure 1: Dry thermal simulation at 1000 s on a 256×128 grid. Perturbational potential temperature (left) is shown with contours every 0.2 K; vertical velocity (right) is shown with contours every $2\,\mathrm{m\ s^{-1}}$. Negative contours are dashed. Contrast to Fig. 1 in [BF02].

Let us consider a uniform grid of 256×128 points, slightly finer than the original 100 m grid spacing in [BF02]. Figure 1 shows the perturbational potential temperature ($\theta' = \theta - \theta_0$) (left)

and the vertical velocity (right) after 1000 s. Very good agreement is found with respect to the solutions in [BF02] in terms of the height and width of the rising thermal. The maximum and minimum values for θ' are given by 2.03970 K and -0.17278 K, respectively, compared with the original 2.07178 K and -0.144409 K in [BF02]. The maximum and minimum values of the velocity in our computation are 14.2118 m s^{-1} and -8.10941 m s^{-1}, respectively, which are very close to 14.5396 m s^{-1} and -8.58069 m s^{-1}, the values presented in [BF02]. For the computations shown here the advective CFL number, based on the velocity but not the sound speed, was set to 0.9, resulting in time steps of around 4.9 s for the dry thermal computations. Performing the same computation with the compressible code described in [DAB$^+$14] and an acoustic CFL number of 0.9 took roughly 6 times more computational time (537 s versus 98 s for the current implementation) because of the difference in time step size.

5.1.2 The Moist Simulation

We consider the same configuration as above, but with a moist atmospheric environment. A neutrally stable environment can be obtained by considering the wet equivalent potential temperature θ_e, defined for a reversible moist adiabatic atmosphere by

$$\theta_e = T \left(\frac{p_a}{p_{00}} \right)^{-R_a/(c_{pa}+c_{pl}r_t)} \exp \left[\frac{L_v r_v}{(c_{pa} + c_{pl} r_t)T} \right], \tag{51}$$

taken from [Ema94]. Supposing that the total water mixing ratio is constant at all levels, the vertical profiles of π, θ, r_v, and r_c can be obtained using (47), (48), and (51), if values for θ_e and r_t are provided. We finally compute the hydrostatic base state written in terms of p_0, T, q_v, and q_l in our formulation. The value of r_t must be greater than $r_{vs} = q_v^*/q_a$, so that the initial environment is saturated, that is, $q_v = q_v^*$ and $q_l > 0$ everywhere in the domain. The initial perturbation (49) is then introduced in such a way that the buoyancy fields are identical in both the dry and moist simulations, when $\theta_0 = 300$ K in the dry case [BF02]. The initial field for θ is thus given by

$$\theta(p,T) \left(1 + \frac{r_{vs}(p,T)}{\epsilon} \right) = \theta_{\rho 0}(1 + r_t) \left(\frac{\theta'}{300} + 1 \right), \tag{52}$$

which is solved for T, point–wise throughout the domain, at constant pressure $p_0(z)$.

We consider the first approach to account for phase transitions. The divergence constraint is thus given by (34) with α and S defined by (25), and the evaporation rate (33). For this particular problem, $\mathcal{H} = 0$ in S, and hence it is not necessary to compute $\mathcal{C}_e$ in (33).

The moist rising thermal is computed with input parameters: $\theta_{e0} = 320$ K and $r_t = 0.02$. For a 256×128 grid, time steps are roughly constant of about 4.3 s, slightly smaller than in the previous dry computation. Introduction of moisture physics involves an additional computational cost of approximately 15 to 20 % with respect to the dry computation. The maximum and minimum values for the perturbational wet equivalent potential temperature ($\theta'_e = \theta_e - \theta_{e0}$) are given by 4.05402 K and -0.28931 K, respectively, compared with the original 4.09521 K and -0.305695 K in [BF02]. Additionally, our computation yields 15.8199 m s^{-1} and -9.45586 m s^{-1}, for the maximum and minimum vertical velocities, respectively, to be compared with 15.7130 m s^{-1} and -9.92698 m s^{-1} in [BF02]. The solutions are practically identical in terms of position, height, and width of the thermal, as seen in Figure 2. Comparing again with the corresponding numerical solution computed with a compressible formulation [DAB$^+$14], the computational time is again about 6 times shorter with the low Mach number model (113 s here as opposed to 623 s for the compressible simulation). Let us now consider the second approach previously derived which does not explicitly estimate e_v, but rather

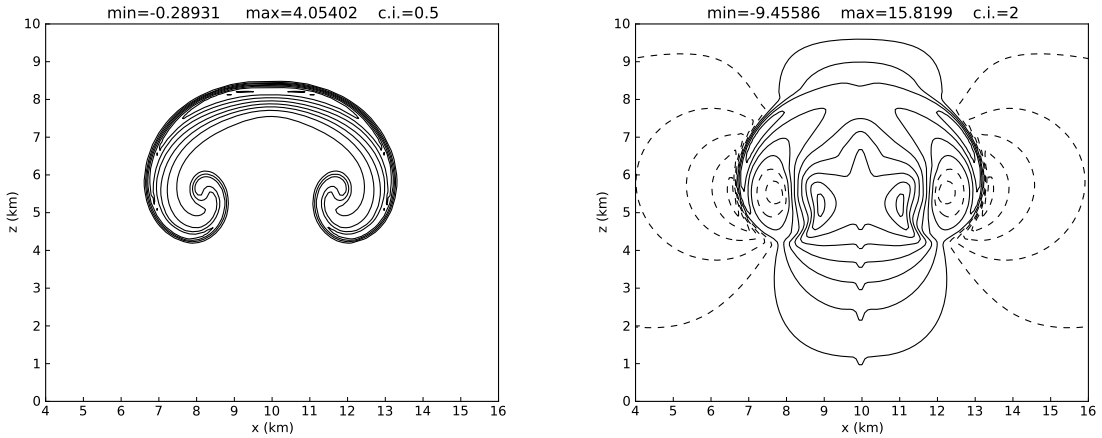

Figure 2: Moist thermal simulation with divergence constraint (34) (first approach) at 1000 s on a 256×128 grid. Perturbational potential temperature (left) is shown with contours every 0.5 K; vertical velocity (right) is shown with contours every 2 m s^{-1}. Negative contours are dashed. Contrast to Fig. 3 in [BF02].

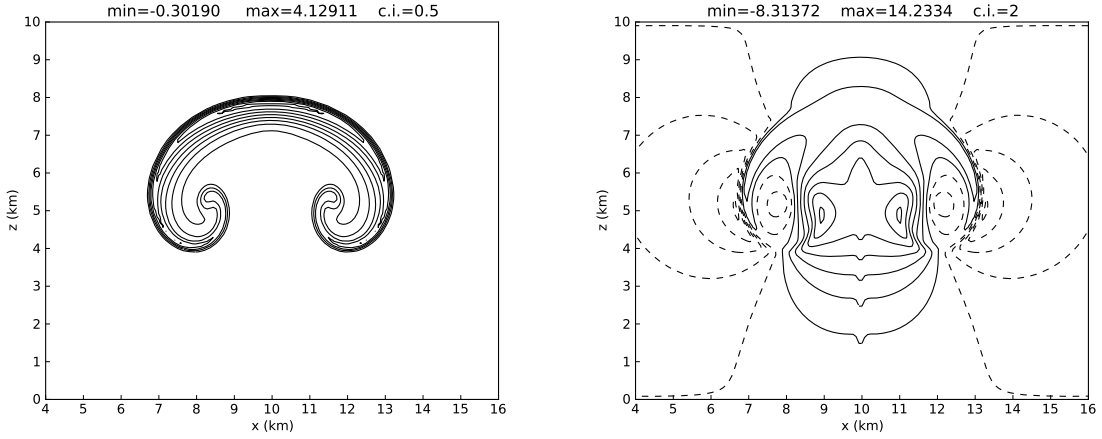

Figure 3: Moist thermal simulation with modified divergence constraint (35) (second approach) at 1000 s on a 256×128 grid. Perturbational potential temperature (left) is shown with contours every 0.5 K; vertical velocity (right) is shown with contours every 2 m s^{-1}. Negative contours are dashed. Contrast to Fig. 3 in [BF02].

considers a modified divergence constraint (eq. (35)) with $\widetilde{\alpha}$ and $\widetilde{S}$ defined by (36). Since for this particular problem, $\mathcal{H} = 0$, we have $\widetilde{S} = 0$.

As before the moist rising thermal is computed with input parameters: $\theta_{e0} = 320$ K and $r_t = 0.02$. For a 256×128 grid, time steps are roughly constant of about 4.8 s, slightly larger than the previous 4.3 s in the first approach. The computational times are roughly 10 to 15 % faster for this configuration. The maximum and minimum values for the perturbational wet equivalent potential temperature ($\theta'_e = \theta_e - \theta_{e0}$) are given by 4.12911 K and -0.30190 K, respectively, compared with the original 4.09521 K and -0.305695 K in [BF02]. Comparing with the previous results in Figure 2, a slight difference in the height of the thermal can be observed. The velocities also have lower maximum values. Increasing the space and time resolution by

considering, for instance, a 512×256 grid improves the quality of the approximations, but it does not eliminate the previous height shift.

5.2 Comparison with compressible simulations

In this part we evaluate the accuracy of the low Mach approach relative to the fully compressible model. We consider a reference compressible solution computed with the fully coupled solver developed in [DAB$^+$14], that solves the compressible Euler equations of motion.

5.2.1 Benchmark problem

We consider again the moist configuration of the benchmark problem in [BF02]. All simulations were carried out on a uniform grid of 512×256. The compressible solution was performed on a finer grid of 1024×512 in order to get a more accurate reference solution.

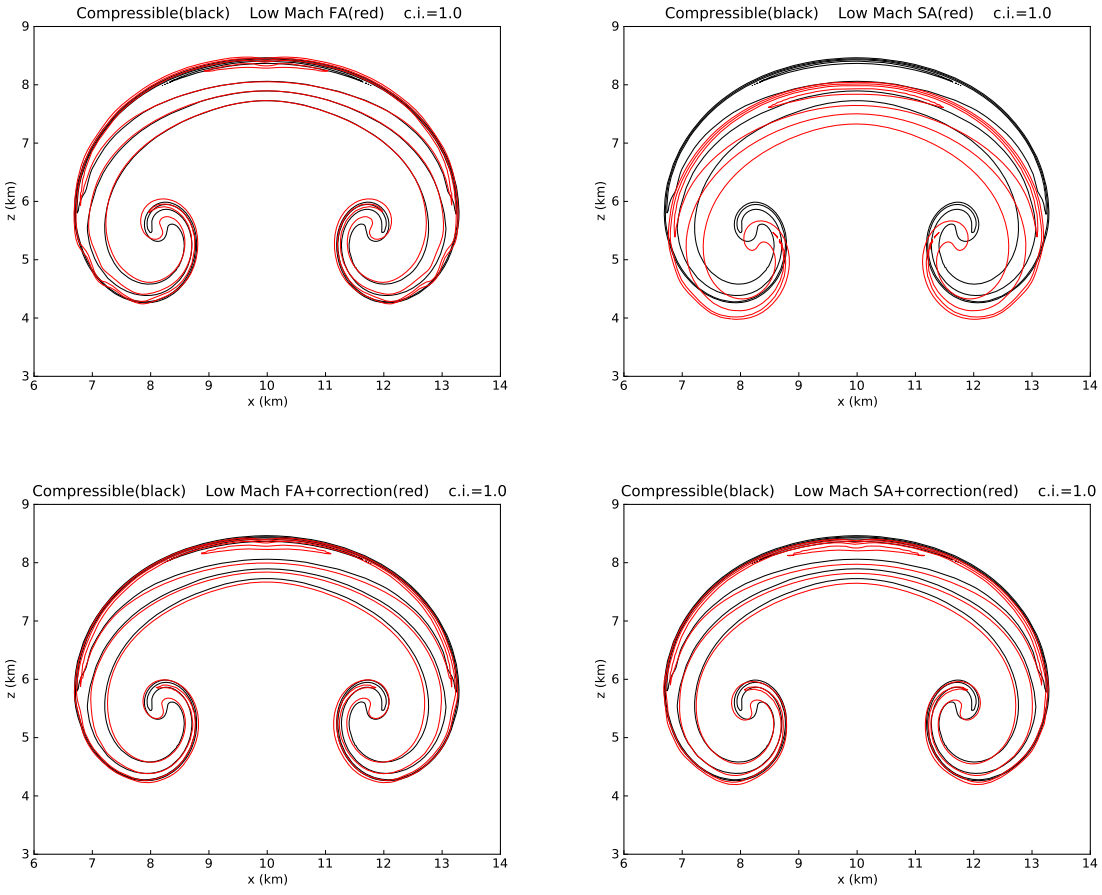

Figure 4: Comparison with the compressible solution for the moist thermal simulations at 1000 s. Perturbational potential temperature is shown with contours every 1 K: first (left) and second approach (right) The simulations in the bottom row include the $\delta\Gamma_1$–correction.

Figure 4 shows computations performed using the low Mach formulation, for θ_0' overlaid on the reference compressible solution. Very good agreement is achieved with the first approach, previously shown in Figure 2, whereas an important height shift can be noticed in the rising thermal given by the second solution, considered in Figure 3. Accounting for the local variation of $\gamma_m(\boldsymbol{x})$ and $\widetilde{\gamma}_m(\boldsymbol{x})$, through the the $\delta\Gamma_1$–correction described in §4, we obtain different results

for both cases. With the first approach very good agreement with the reference solution is still observed, where in particular the thermal tips are slightly better approximated; however, a slight height deficit can also be observed. The introduction of the $\delta\Gamma_1$–correction considerably improves the second approximation. As a matter of fact, while averaging $\gamma_m(\boldsymbol{x})$ involves neglecting local variations that range from -8×10^{-5} to 6.5×10^{-4} in the first case; the latter values become -6.7×10^{-3} and 1.5×10^{-3} for the averaged $\widetilde{\gamma}_m(\boldsymbol{x})$ in the second one. In particular with the $\delta\Gamma_1$–correction, both approaches yield practically the same results.

5.2.2 Non–isentropic Background State

Next, we consider the hydrostatically balanced profiles in [CF84] (eq. 2) for the background state:

$$\left.\begin{aligned}\theta_0(z) &= \theta_{00}\exp(Sz),\\ p_0(z) &= p_{00}\left[1-\frac{g}{c_{pa}\theta_{00}S}\left(1-\exp(-Sz)\right)\right]^{c_{pa}/R_a},\end{aligned}\right\} \tag{53}$$

where θ_{00} and p_{00} stand for the environmental potential temperature and pressure at the surface ($z=0$), with the static stability S defined as $S=N^2/g=d\ln\theta_0/dz$ (N is the Brunt–Väisälä frequency). The potential temperature is given by (46). For the following computations we define a computational domain 4 km high and wide, with periodic horizontal boundary conditions. Zero normal velocities are imposed at vertical boundaries, while the remaining variables are extrapolated to determine the corresponding fluxes. The same thermodynamic parameters from [BF02] are considered, whereas constants (28) coming from [Rom08] are considered in the Clausius–Clapeyron equation (27) with $p_{\text{trip}}=611\,\text{Pa}$. From [GC91], we take $S=1.3\times10^{-5}\,\text{m}^{-1}$, $\theta_{00}=283\,\text{K}$, and $p_{00}=850\,\text{hPa}$. All simulations with the low Mach formulation were performed on a uniform grid of 256×256. As before, the reference compressible solutions were computed on a finer grid of 1024×1024.

With our formulation we also need to compute the hydrostatic base density ρ_0 based on the background temperature and pressure (53), and the distribution of air, water vapor, and liquid water in the atmosphere. The latter quantities are set by the relative humidity in the atmosphere, RH, measured in percentage and defined as $\text{RH}=(p_v/p_v^*)\times100$. In particular if $\text{RH}_0<100\,\%$, then no liquid water should be initially present in the atmosphere in order to guarantee the thermodynamic equilibrium of the initial state, that is, $q_{l0}(z)=0$. Following [DAB+14], we consider in this study two cases: first, a saturated medium, that is $\text{RH}_0=100\,\%$ and $r_t=0.02$, just like in the moist benchmark problem; and a second configuration with $\text{RH}_0=20\,\%$, and hence, no liquid water in the initial background state. Contrary to the benchmark configuration in [BF02], we now have in either case a non–isentropic background state, where the following definitions of specific entropy have been adopted [Rom08]:

$$\begin{aligned}s_a &= c_{pa}\log\left(\frac{T}{T_{\text{trip}}}\right)-R_a\log\left(\frac{p}{p_{\text{trip}}}\right),\\ s_v &= c_{pv}\log\left(\frac{T}{T_{\text{trip}}}\right)-R_v\log\left(\frac{p}{p_{\text{trip}}}\right)+S_{0v},\\ s_l &= c_{vl}\log\left(\frac{T}{T_{\text{trip}}}\right),\\ s_m &= q_a s_a+q_v s_v+q_l s_l,\end{aligned} \tag{54}$$

for dry air, water vapor, liquid water, and moist air, with $S_{0v}=E_{0v}/T_{\text{trip}}+R_v$.

Let us consider the first configuration with an initially saturated environment. Similar to (49), we introduce a warm perturbation of temperature:

$$T' = 2\cos^2\left(\frac{\pi L}{2}\right), \tag{55}$$

where L is defined by (50), with $x_c = 2\,\mathrm{km}$, $z_c = 0.8\,\mathrm{km}$, and $x_r = z_r = 300\,\mathrm{m}$. The water distributions, as well as the density, are thus adjusted to the perturbed temperature with the original pressure field. Figure 5 shows solutions obtained with the low Mach formulation using the first and second approach for the divergence constraint, as well as the compressible reference solution. Solutions are very similar in all three cases even though the low Mach approximations yield thermals rising slightly faster. Introducing the $\delta\Gamma_1$–correction does not change the results much. The deviation of $\gamma_m(\boldsymbol{x})$ from $\overline{\gamma}_m(z)$ in the first approach ranges from 0 to 2.5×10^{-3}; the deviation of $\widetilde{\gamma}_m(\boldsymbol{x})$ from $\overline{\widetilde{\gamma}}_m(z)$ in the second approach ranges from -10^{-2} to 0. For a 256×256 grid and a CFL factor of 0.9, the time steps for the low Mach approximations are of about 1.4 s compared to 0.04 s with the compressible formulation. The low Mach number simulation takes roughly a factor of 13 less computational time than the compressible simulation.

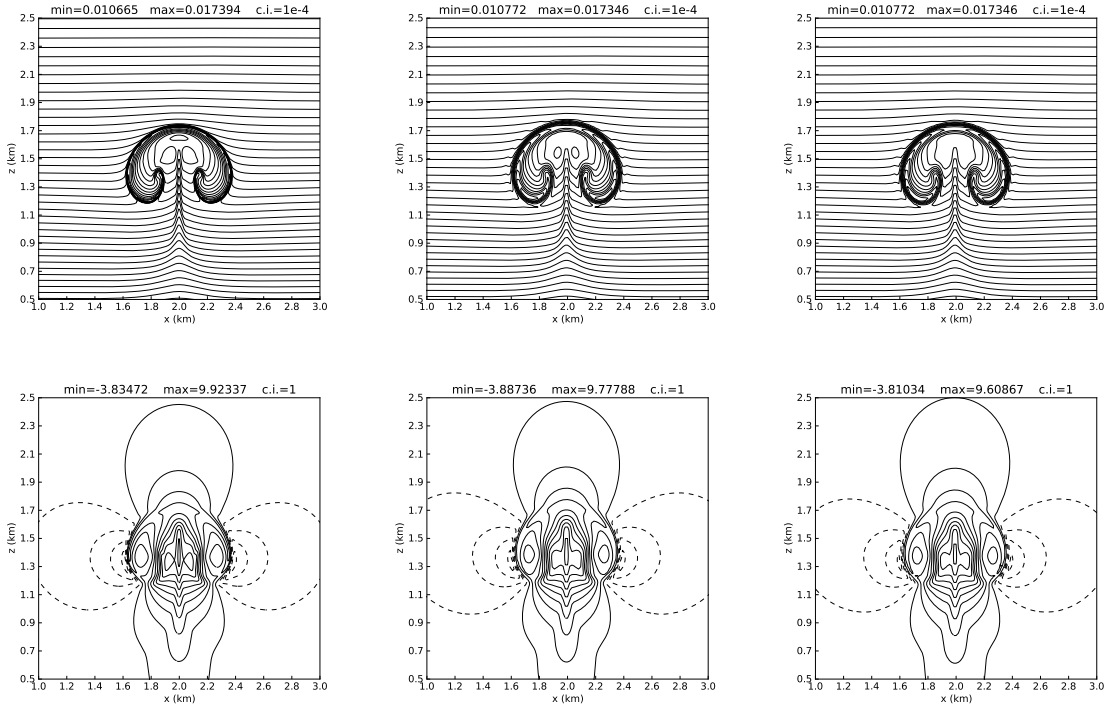

Figure 5: Initially saturated, non–isentropic background state. Liquid water mass fraction (top) and vertical velocity (bottom) are shown for the reference compressible (left), and low Mach number solution at 300 s using the first (center) and second (right) approach. Contours are every 10^{-4} (top) and $1\,\mathrm{m\ s^{-1}}$ (bottom); negative contours are dashed.

For the second configuration with $\mathrm{RH}_0 = 20\,\%$, we consider the same temperature perturbation (55) and an additional circular perturbation on the relative humidity, which is set to 100 % for a radius $r < 200\,\mathrm{m}$, as considered in [GC91]. A transition layer is assumed such that

$$\mathrm{RH} = \mathrm{RH}_0 + (100 - \mathrm{RH}_0)\cos^2\left(\frac{\pi}{2}\frac{r - 200}{100}\right),\ 200 \le r \le 300, \tag{56}$$

taken also from [GC91]. Initially there is no liquid water in the domain. The perturbed water vapor is computed based on (55) and (56) with the original base state pressure. Like Figure 4, Figure 6 compares the two low Mach number solutions to the reference compressible solution. In this case, the $\delta\Gamma_1$–correction must be taken into account if the modified divergence constraint (35) is used (second approach). Here the deviation of $\gamma_m(\boldsymbol{x})$ from $\overline{\gamma}_m(z)$ in the first approach ranges from -4.2×10^{-3} to 6.9×10^{-4}, which is considerably smaller than the deviation of $\widetilde{\gamma}_m(\boldsymbol{x})$ from $\overline{\widetilde{\gamma}}_m(z)$ in the second approach, which ranges from -0.17 to 3.3×10^{-2}.

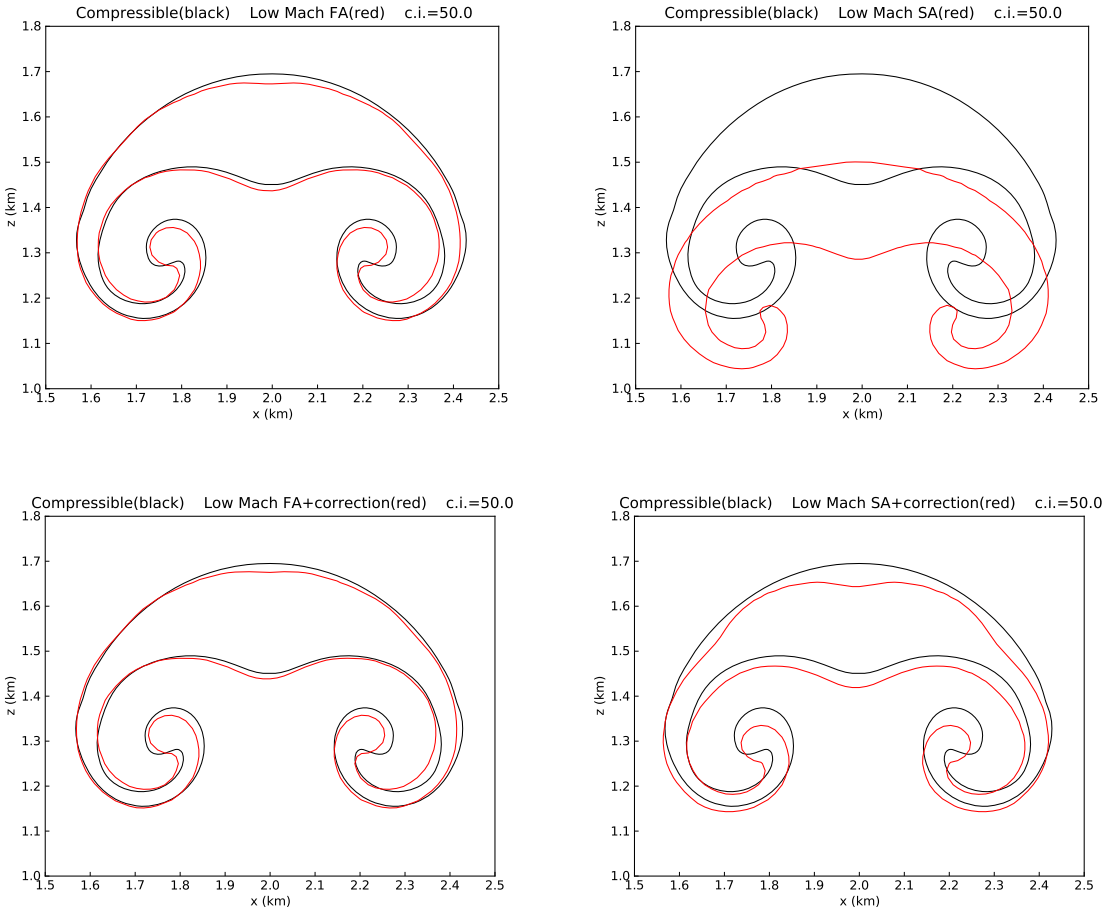

Figure 6: Non–isentropic background state with a saturated perturbation. Moist specific entropy (54) is shown with contours every 50 J kg^{-1} K^{-1}. The low Mach number solution at 300 s (red) using the first (left) and second (right) approach overlays the reference compressible solution (black). On the bottom are simulations that use the $\delta\Gamma_1$–correction.

Better agreement can be seen in Figure 7, where the term of order $\delta\Gamma_1^2$ is also considered in (42) for the $\delta\Gamma_1$–correction:

$$\boldsymbol{\nabla} \cdot \boldsymbol{U} = -\frac{1}{\overline{\Gamma}_1 p_0} \frac{Dp_0}{Dt} + S + \frac{\delta\Gamma_1}{\overline{\Gamma}_1^2 p_0} \frac{Dp_0}{Dt} - \frac{\delta\Gamma_1^2}{\overline{\Gamma}_1^3 p_0} \frac{Dp_0}{Dt}. \tag{57}$$

Time steps used in the low Mach computations are of about 2.1 s, compared to 0.04 s with the compressible formulation. Total computational times are reduced by a factor of about 15.

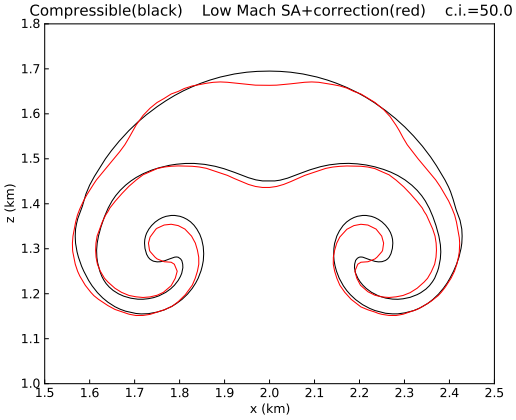

Figure 7: Non–isentropic background state with a saturated perturbation. Moist specific entropy (54) is shown with contours every 50 J kg^{-1} K^{-1}. The low Mach solution at 300 s (red) using the $\delta\Gamma_1$–correction given by (57) overlays the reference compressible solution (black).

5.2.3 Three–dimensional simulation

Finally, we consider two interacting thermals rising in a three–dimensional, non–isentropically stratified background in a domain 10 km on a side and 15 km high. The background state is defined as in §5.2.2 with the formulas in (53) and the same constants used. The background has a relative humidity of $\mathrm{RH}_0 = 20\,\%$ and no liquid water is present in the initial configuration. The following temperature perturbation is then introduced:

$$T' = 6\cos^2\left(\frac{\pi L_1}{2}\right) + 6\cos^2\left(\frac{\pi L_2}{2}\right), \tag{58}$$

where $L_1 = \min(1, r_1)$, $L_2 = \min(1, r_2)$, and

$$r_1 = \frac{1}{4}\sqrt{(x-x_1)^2 + (y-y_1)^2 + (z-z_1)^2}\,, \tag{59}$$

$$r_2 = \frac{1}{3}\sqrt{(x-x_2)^2 + (y-y_2)^2 + (z-z_2)^2}, \tag{60}$$

with $x_1 = y_1 = 5$ km, $z_1 = 7.5$ km and $x_2 = y_2 = 7$ km, $z_2 = 7.5$ km. Within the regions where the temperature is perturbed, we also perturb the relative humidity by setting RH equal to 50 % for $r_1 < 3$ km and $r_2 < 2$ km, for each initial thermal, with corresponding transition layers:

$$\mathrm{RH} = \mathrm{RH}_0 + (50 - \mathrm{RH}_0)\cos^2\left(\frac{\pi}{2}\,[r_1 - 3]\right),\ 3 \le r_1 \le 4, \tag{61}$$

$$\mathrm{RH} = \mathrm{RH}_0 + (50 - \mathrm{RH}_0)\cos^2\left(\frac{\pi}{2}\,[r_2 - 2]\right),\ 2 \le r_2 \le 3. \tag{62}$$

We consider the low Mach number formalism using the second approach (modified divergence constraint (35)) to numerically implement phase transitions, with the $\delta\Gamma_1$–correction given by (57). As before, the low Mach number solutions are contrasted to reference compressible solutions. For a uniform grid of size $256 \times 256 \times 384$, the time step in the low Mach number simulation is approximately 3 s, compared to 0.1 s in the compressible simulation. For this particular problem, the total run time of the low Mach number simulation is roughly

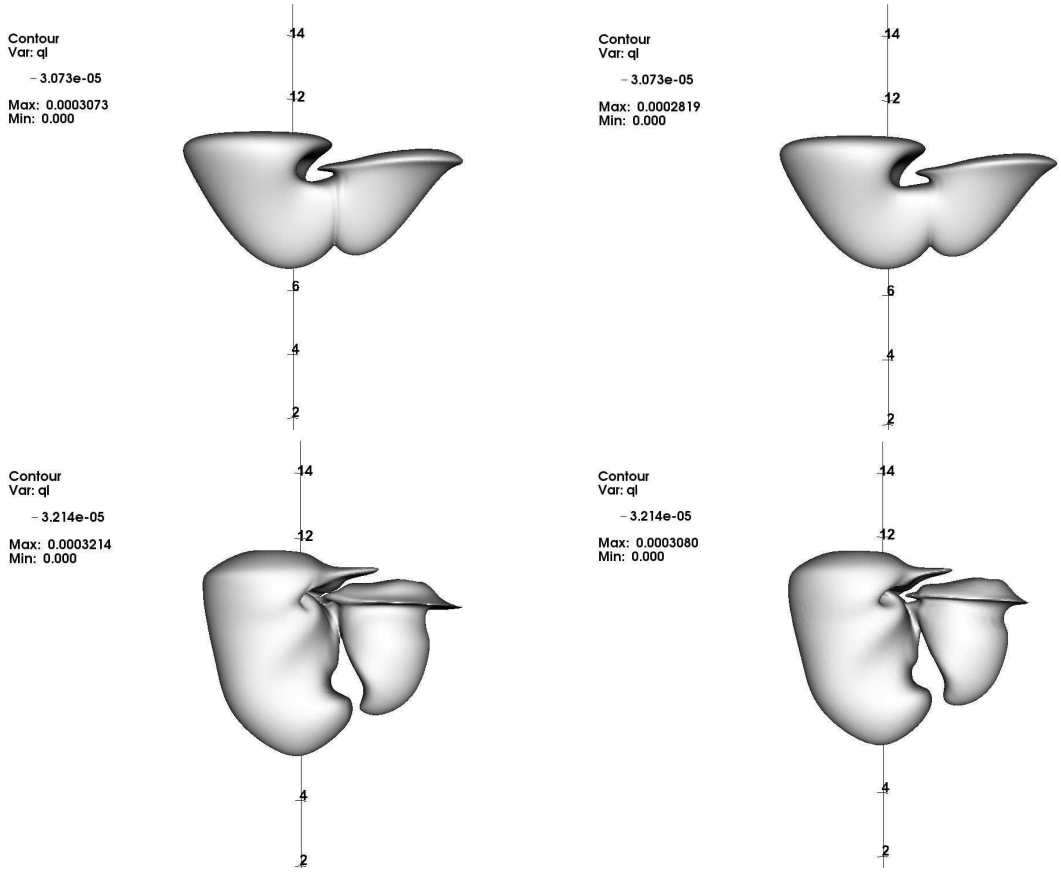

Figure 8: Two interacting thermals in a three–dimensional non–isentropic background state. Isosurfaces of liquid water for the reference compressible solutions (left) and the low Mach number ones (right) at times 500 s ($q_l = 3.073 \times 10^{-5}$) (top) and 1000 s (bottom) ($q_l = 3.214 \times 10^{-5}$). The low Mach number solver uses the modified divergence constraint (35) (second approach) with the $\delta\Gamma_1$–correction given by (57).

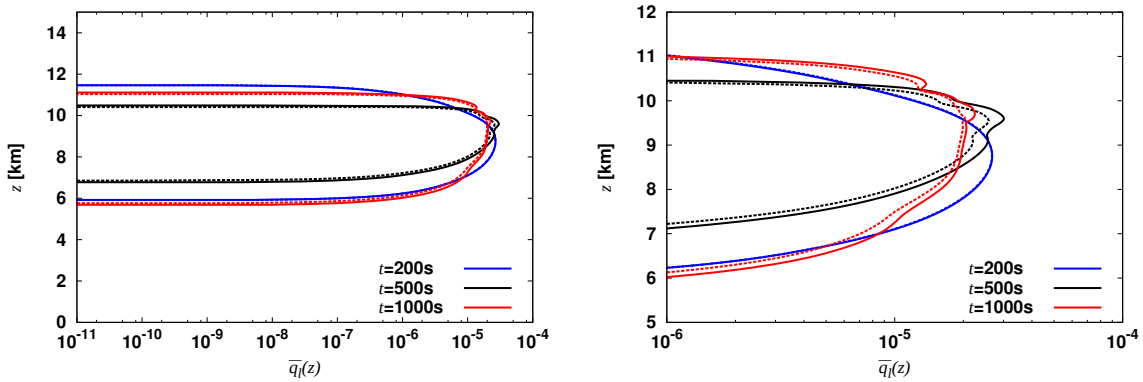

Figure 9: Horizontal budgets of liquid water, $\overline{q_l}(z)$, computed with (37) at $t = 200$ s, 500 s and 1000 s. Reference compressible and low Mach number solutions are represented with solid and dashed lines, respectively. More details can be appreciated in the zoomed region (right).

a factor of 5 less than that of the compressible simulation. Figure 8 illustrates the formation of liquid water as computed with both formulations. The relative difference between the

maximum values of q_l in the compressible and the low Mach number solutions is roughly 8 % at $t = 500\,\mathrm{s}$ and 4 % at $t = 1000\,\mathrm{s}$, the two times shown in Figure 8. Figure 9 shows the horizontal budgets of liquid water, $\overline{q_l}(z)$, computed using formula (37), at $t = 200\mathrm{s}$ and at the two simulation times shown in Figure 8. For $t = 200\,\mathrm{s}$ practically the same solution is recovered with both formulations, with a relative difference of 0.2 % between the maximum values of q_l. Recalling that q_l is diagnostically recovered in both the compressible and the low Mach number approach, we can track the formation of liquid water by computing it after each time step for comparison purposes. Local values of q_l larger than 10^{-10} appear after 111 s and 112.5 s for the compressible and low Mach number simulations, respectively. The Mach number M associated with this particular problem remains lower than 0.05 during the entire numerical simulation.

6 Summary

We have presented a new low Mach number model for moist atmospheric flows with a general equation of state, based on the low Mach number model for stratified reacting flows introduced in [ABNZ08]. In our model we consider only reversible processes, namely water phase changes as in [OK14], using an exact Clausius–Clapeyron formula for moist thermodynamics and considering the effects of the specific heats of water and the temperature dependency of the latent heat. A set of invariant variables was used as prognostic variables in the equations of motion, including in particular the total water content and a specific enthalpy of moist air that accounts for the contribution of both sensible and latent heats. The evolution equations can thus be solved without needing to estimate or neglect source terms related to phase change during the time integration. The mass fractions of water vapor and liquid water are diagnostically recovered as required during a time step by imposing the saturation requirements of an atmosphere at thermodynamic equilibrium. The latter is an important property since updating the solution while ignoring the varying water composition, may negatively impact the accuracy of the moist flow dynamics, as investigated in [DAB$^+$14].

We then considered a moist thermodynamic model that treats dry air and water vapor as ideal gases to define the equation of state for moist air. In order to account for the latent heat release in the low Mach divergence constraint for the velocity field, the evaporation rate is estimated from the time variation of saturated water vapor within a parcel. The amount of saturated water vapor within a parcel is determined by the Clausius–Clapeyron formula as a function of the local thermodynamical state; the evolution of the state depends on the local advected motions. An analytical expression for the evaporation rate was thus derived that depends on local parameters given by the temperature and pressure, the water composition, and the velocity field. Two approaches were then considered. In the first, the rate of phase change can be computed to evaluate the latent heat release; in the second, a modified divergence constraint can be analytically deduced by introducing the derived expression for the evaporation rate in the original divergence constraint. Both approaches are analytically equivalent and together with the low Mach number equation set allow us to characterize moist atmospheric flows.

The MAESTRO code[1] [NAB$^+$10], originally designed to simulate stratified reacting flows arising in astrophysical settings, was adapted to model moist atmospheric flows. A series of test problems was investigated with both isentropic and non–isentropic background states, as well as saturated and partially saturated regions in the atmosphere. Results were contrasted to reference solutions obtained with a fully compressible formulation. Very good agreement with the reference moist dynamics was shown using both the first and second approach (with the

[1] Available at http://bender.astro.sunysb.edu/Maestro/download/

$\delta\Gamma_1$–correction), thus demonstrating that low Mach number models can serve as a reasonably accurate and computationally efficient alternative to compressible codes for small-scale moist atmospheric applications.

Acknowledgments

This material is based upon work supported by the U.S. Department of Energy, Office of Science, Office of Advanced Scientific Computing Research, Applied Mathematics program under contract number DE-AC02005CH11231.

A Derivation of the low Mach divergence constraint

We rewrite the conservation of mass (eq. (1)) as an expression for the divergence of velocity,

$$\boldsymbol{\nabla}\cdot\boldsymbol{U} = -\frac{1}{\rho}\frac{D\rho}{Dt}. \tag{63}$$

Differentiating the equation of state, written as $p = p(\rho, T, q_a, q_v, q_l)$, along particle paths, we obtain

$$\begin{aligned}\frac{D\rho}{Dt} &= \frac{1}{p_\rho}\left(\frac{Dp}{Dt} - p_T\frac{DT}{Dt} - \sum_{i\in(a,v,l)} p_{q_i}\frac{Dq_i}{Dt}\right)\\ &= \frac{1}{p_\rho}\left(\frac{Dp}{Dt} - p_T\frac{DT}{Dt} - \left(p_{q_v} - p_{q_l}\right)\frac{e_v}{\rho}\right),\end{aligned} \tag{64}$$

with $p_\rho = \partial p/\partial\rho|_{T,q_i}$, $p_T = \partial p/\partial T|_{\rho,q_i}$, and $p_{q_i} = \partial p/\partial q_i|_{\rho,T,(q_j,j\neq i)}$. An expression for DT/Dt can be obtained by differentiating the definition of moist enthalpy (eq. (9)), and comparing terms with the enthalpy equation (3):

$$\begin{aligned}\rho\frac{D\widehat{h}}{Dt} &= \rho\left(\left.\frac{\partial\widehat{h}}{\partial T}\right|_{p,q_i}\frac{DT}{Dt} + \left.\frac{\partial\widehat{h}}{\partial p}\right|_{T,q_i}\frac{Dp}{Dt} + \sum_{i\in(a,v,l)}\left.\frac{\partial\widehat{h}}{\partial q_i}\right|_{T,p,(q_j,j\neq i)}\frac{Dq_i}{Dt}\right)\\ &= \rho\left(c_{pm}\frac{DT}{Dt} + \widehat{h}_p\frac{Dp}{Dt} + \left(\widehat{h}_{q_v} - \widehat{h}_{q_l}\right)\frac{e_v}{\rho}\right)\\ &= \frac{Dp}{Dt} + \rho\mathcal{H},\end{aligned} \tag{65}$$

or, gathering terms,

$$\frac{DT}{Dt} = \frac{1}{\rho c_{pm}}\left[\left(1 - \rho\widehat{h}_p\right)\frac{Dp}{Dt} - \left(\widehat{h}_{q_v} - \widehat{h}_{q_l}\right)e_v + \rho\mathcal{H}\right], \tag{66}$$

where $c_{pm} = \partial\widehat{h}/\partial T|_{p,q_i}$ is the specific heat of moist air at constant pressure, $\widehat{h}_p = \partial\widehat{h}/\partial p|_{T,q_i}$, and $\widehat{h}_{q_i} = \partial\widehat{h}/\partial q_i|_{T,p,(q_j,j\neq i)}$. Coming back to equation (63) and replacing p by $p_0(z,t)$, we can write the divergence constraint on the velocity field as (14) with α and S given by (15).

B Derivation of the evaporation rate

Considering that $e_v = \rho Dq_v^*/D_t$ from (32) and differentiating $q_v^* = q_v^*(\rho, T)$ (eq. (29)) along particle paths, we obtain

$$e_v = \rho\left[\left.\frac{\partial q_v^*}{\partial\rho}\right|_T\frac{D\rho}{Dt} + \left.\frac{\partial q_v^*}{\partial T}\right|_\rho\frac{DT}{Dt}\right], \tag{67}$$

with

$$\left.\frac{\partial q_v^*}{\partial \rho}\right|_T = -\frac{q_v^*}{\rho}, \qquad \left.\frac{\partial q_v^*}{\partial T}\right|_\rho = q_v^*\left(\frac{\alpha_v - 1}{T} + \frac{\beta_v}{T^2}\right) = q_v^*\phi(T), \tag{68}$$

according to (29) and (27). With the equation of state (23), equation (66) becomes

$$\frac{DT}{Dt} = \frac{1}{\rho c_{pm}}\left[\frac{Dp}{Dt} - L_e e_v + \rho\mathcal{H}\right], \tag{69}$$

and hence,

$$e_v = \frac{q_v^*\left[\rho c_{pm}\left(\boldsymbol{\nabla}\cdot\boldsymbol{U}\right) + \phi(T)\left(\frac{Dp}{Dt} + \rho\mathcal{H}\right)\right]}{c_{pm} + q_v^*\phi(T)L_e}; \tag{70}$$

that is,

$$\mathcal{A}_e = \frac{q_v^*\rho c_{pm}}{c_{pm} + q_v^*\phi(T)L_e}, \qquad \mathcal{B}_e = \frac{q_v^*\phi(T)}{c_{pm} + q_v^*\phi(T)L_e}, \qquad \mathcal{C}_e = \frac{q_v^*\phi(T)}{c_{pm} + q_v^*\phi(T)L_e}, \tag{71}$$

into (33) replacing also p by $p_0(z,t)$.

Notice that another expression for e_v can be derived considering $q_v^* = q_v^*(q_a, p, T)$ (eq. (30)) in $e_v = \rho D q_v^*/D_t$. Moreover, two more expressions for e_v can be found using

$$\frac{DT}{Dt} = \frac{1}{\rho c_{vm}}\left[-p\left(\boldsymbol{\nabla}\cdot\boldsymbol{U}\right) - (L_e - R_v T)e_v + \rho\mathcal{H}\right], \tag{72}$$

instead of (69), deduced from the conservation equation for internal energy $\widehat{e}$ instead of enthalpy $\widehat{h}$. Numerical computations using different formulations for e_v yield practically identical results.

C Modified divergence constraint

Rearranging terms in (34), after having introduced the estimate of e_v (eq. (33)) in S (eq. (25)), yields the modified divergence constraint (35) with

$$\widetilde{\alpha} = \frac{\dfrac{1}{\gamma_m p_0} - \dfrac{\mathcal{B}_e}{\rho}\left[\dfrac{1}{(\epsilon q_a + q_v)} - \dfrac{L_e}{c_{pm}T}\right]}{1 - \dfrac{\mathcal{A}_e}{\rho}\left[\dfrac{1}{(\epsilon q_a + q_v)} - \dfrac{L_e}{c_{pm}T}\right]}, \tag{73}$$

$$\widetilde{S} = \frac{\left[\dfrac{1}{c_{pm}T}\right]\mathcal{H} + \mathcal{C}_e\left[\dfrac{1}{(\epsilon q_a + q_v)} - \dfrac{L_e}{c_{pm}T}\right]\mathcal{H}}{1 - \dfrac{\mathcal{A}_e}{\rho}\left[\dfrac{1}{(\epsilon q_a + q_v)} - \dfrac{L_e}{c_{pm}T}\right]} = \widetilde{\sigma}\mathcal{H}; \tag{74}$$

and thus

$$\widetilde{\sigma} = \frac{\rho\left\{(\epsilon q_a + q_v) + \mathcal{C}_e\left[c_{pm}T - (\epsilon q_a + q_v)L_e\right]\right\}}{(\epsilon q_a + q_v)\rho c_{pm}T - \mathcal{A}_e\left[c_{pm}T - (\epsilon q_a + q_v)L_e\right]}. \tag{75}$$

After some manipulation, we can write that $\widetilde{\alpha} = 1/(\widetilde{\gamma}_m p_0)$ with

$$\widetilde{\gamma}_m = \gamma_m\left[\frac{1 + c_{vm}\Phi}{1 + R_m T\phi(T)\Phi}\right], \qquad \Phi = \frac{q_v^*\left[R_m L_e - c_{pm}R_v T\right]}{c_{vm}R_m T\left[c_{pm} + q_v^*\phi(T)L_e\right]}, \tag{76}$$

using (71). In particular if there is no phase transition ($e_v = 0$), then $\Phi = 0$ and $\widetilde{\gamma}_m = \gamma_m$; similarly, $\mathcal{A}_e = \mathcal{C}_e = 0$ in (75) and $\widetilde{\sigma} = \sigma$.

As pointed out in Appendix B, three more expressions for e_v, other than (70), can be derived yielding four different formulations for $\widetilde{\alpha}$ and $\widetilde{S}$ in the modified divergence constraint (35). Nevertheless, all of them yield practically identical numerical results.

References

[ABNZ] A. S. Almgren, J. B. Bell, A. Nonaka, and M. Zingale. On new low Mach number equations for stratified flows. *In preparation.*

[ABNZ08] A. S. Almgren, J. B. Bell, A. Nonaka, and M. Zingale. Low Mach number modeling of Type Ia supernovae. III. Reactions. *ApJ*, 684:449–470, 2008.

[ABRZ06a] A. S. Almgren, J. B. Bell, C. A. Rendleman, and M. Zingale. Low Mach number modeling of Type Ia supernovae. I. Hydrodynamics. *ApJ*, 637:922–936, 2006.

[ABRZ06b] A. S. Almgren, J. B. Bell, C. A. Rendleman, and M. Zingale. Low Mach number modeling of Type Ia supernovae. II. Energy evolution. *ApJ*, 649:927–938, 2006.

[Alm00] A. S. Almgren. A new look at the pseudo-incompressible solution to Lamb's problem of hydrostatic adjustment. *J. Atmos. Sci.*, 57:995–998, April 2000.

[Bat53] G. K. Batchelor. The conditions for dynamical similarity of motions of a frictionless perfect-gas atmosphere. *Q. J. R. Meteorol. Soc.*, 79:224–235, 1953.

[Bet73] A. K. Betts. Non–precipitating cumulus convection and its parameterization. *Q. J. R. Meteorol. Soc.*, 99(419):178–196, 1973.

[BF02] G. H. Bryan and J. M. Fritsch. A benchmark simulation for moist nonhydrostatic numerical models. *Mon. Wea. Rev.*, 130:2917–2928, 2002.

[CF84] T. L. Clark and R. D. Farley. Severe downslope windstorm calculations in two and three spatial dimensions using anelastic interactive grid nesting: A possible mechanism for gustiness. *J. Atmos. Sci.*, 41:329–350, 1984.

[Cla79] T. L. Clark. Numerical simulations with a three-dimensional cloud model: Lateral boundary condition experiments and multicellular severe storm simulations. *J. Atmos. Sci.*, 36:2191–2215, 1979.

[DAB+14] M. Duarte, A. S. Almgren, K. Balakrishnan, J. B. Bell, and D. M. Romps. A numerical study of methods for moist atmospheric flows: Compressible equations. *To appear in Mon. Wea. Rev.*, 2014.

[DF69] J. A. Dutton and G. H. Fichtl. Approximate equations of motion for gases and liquids. *J. Atmos. Sci.*, 26:241–254, 1969.

[Dur89] D. R. Durran. Improving the anelastic approximation. *J. Atmos. Sci.*, 46(11):1453–1461, 1989.

[Ema94] K. A. Emanuel. *Atmospheric Convection.* Oxford University Press, 1994.

[GC91] W. W. Grabowski and T. L. Clark. Cloud-environment interface instability: Rising thermal calculations in two spatial dimensions. *J. Atmos. Sci.*, 48:527–546, 1991.

[Gou69] D. O. Gough. The anelastic approximation for thermal convection. *J. Atmos. Sci.*, 26:448–456, 1969.

[GS90] W. W. Grabowski and P. K. Smolarkiewicz. Monotone finite-difference approximations to the advection-condensation problem. *Mon. Wea. Rev.*, 118:2082–2097, 1990.

[GS02] W. W. Grabowski and P. K. Smolarkiewicz. A multiscale anelastic model for meteorological research. *Mon. Wea. Rev.*, 130:939–956, 2002.

[HH89] T. Hauf and H. Höller. Entropy and potential temperature. *J. Atmos. Sci.*, 44:2887–2901, 1989.

[KP12] R. Klein and O. Pauluis. Thermodynamic consistency of a pseudoincompressible approximation for general equations of state. *J. Atmos. Sci.*, 69:961–968, 2012.

[KSD07] J. B. Klemp, W. C. Skamarock, and J. Dudhia. Conservative split-explicit time integration methods for the compressible nonhydrostatic equations. *Mon. Wea. Rev.*, 135:2897–2913, 2007.

[KW78] J. B. Klemp and R. B. Wilhelmson. The simulation of three-dimensional convective storm dynamics. *J. Atmos. Sci.*, 35:1070–1096, 1978.

[LH82] F. Lipps and R. Hemler. A scale analysis of deep moist convection and some related numerical calculations. *J. Atmos. Sci.*, 39:2192–2210, 1982.

[NAB+10] A. Nonaka, A. S. Almgren, J. B. Bell, M. J. Lijewski, C. Malone, and M. Zingale. MAESTRO: An adaptive low Mach number hydrodynamics algorithm for stellar flows. *ApJS*, 188:358–383, 2010.

[OK14] W. P. O'Neill and R. Klein. A moist pseudo-incompressible model. *Atmos. Res.*, 142:133–141, 2014.

[Ooy90] K. V. Ooyama. A thermodynamic foundation for modeling the moist atmosphere. *J. Atmos. Sci.*, 47:2580–2593, 1990.

[OP62] Y. Ogura and N. A. Phillips. Scale analysis of deep and shallow convection in the atmosphere. *J. Atmos. Sci.*, 19:173–179, 1962.

[Rom08] D. M. Romps. The dry-entropy budget of a moist atmosphere. *J. Atmos. Sci.*, 65:3779–3799, 2008.

[Sat03] M. Satoh. Conservative scheme for a compressible nonhydrostatic model with moist processes. *Mon. Wea. Rev.*, 131:1033–1050, 2003.

[SO73] S.-T. Soong and Y. Ogura. A comparison between axisymmetric and slab-symmetric cumulus cloud models. *J. Atmos. Sci.*, 30:879–893, 1973.

[TC81] G. J. Tripoli and W. R. Cotton. The use of lce-liquid water potential temperature as a thermodynamic variable in deep atmospheric models. *Mon. Wea. Rev.*, 109:1094–1102, 1981.

[TW76] M. C. Tapp and P. W. White. A non-hydrostatic mesoscale model. *Q. J. Roy. Meteor. Soc.*, 102(432):277–296, 1976.

[VLB+13] G. M. Vasil, D. Lecoanet, B. P. Brown, T. S. Wood, and E. G. Zweibel. Energy conservation and gravity waves in sound-proof treatments of stellar interiors. II. Lagrangian constrained analysis. *ApJ*, 773(2):169, 2013.

[WS98] L. J. Wicker and W. C. Skamarock. A time-splitting scheme for the elastic equations incorporating second-order Runge–Kutta time differencing. *Mon. Wea. Rev.*, 126:1992–1999, 1998.